Combining Theory and Experiment to Interpret the EPR Spectra of VO^{2+}-Exchanged Zeolites

Patrick J. Carl,[†] Sara L. Isley, and Sarah C. Larsen*

Department of Chemistry, University of Iowa, Iowa City, Iowa 52242

Received: February 16, 2001

The electron paramagnetic resonance (EPR) spectra of VO^{2+}-exchanged zeolites were interpreted by comparing theoretical calculations of the EPR parameters for VO^{2+} model complexes with experimental EPR data. This is the first report in which density functional theory (DFT) has been used to calculate the EPR parameters in order to reproduce an empirical correlation between the electronic **g**-factor and the nuclear hyperfine coupling constant, **A**. In this study, a series of VO^{2+}-exchanged zeolites (ZSM5, mordenite, Beta and Y) were prepared by a standard aqueous ion exchange procedure. EPR spectra of the samples were obtained before and after dehydration and in the presence of ammonia. The EPR parameters were determined by applying a least-squares fitting routine to the data. The EPR spectra of the hydrated VO^{2+}-exchanged zeolites exhibited similar EPR spectral features that were independent of the identity of the parent zeolite. After dehydration, the EPR spectra were broad relative to the EPR spectra of the hydrated VO^{2+}-exchanged zeolites, presumably due to site heterogeneity, but otherwise exhibited similar EPR parameters. Upon adsorption of ammonia, the EPR parameters systematically changed; $\mathbf{g}_{||}$ increased and $\mathbf{A}_{||}(^{51}\mathbf{V})$ decreased relative to the EPR parameters for the hydrated VO^{2+}-exchanged zeolites. To further understand ligand binding in this system, the **g** and **A** tensors for several vanadyl model complexes, $VO(H_2O)_4^{2+}$, $VO(H_2O)_5^{2+}$, cis and trans $VO(NH_3)_2(H_2O)_2^{2+}$, $VO(NH_3)_4^{2+}$, and $VO(NH_3)_4H_2O^{2+}$ were calculated using the Amsterdam density functional theory (ADF) program. The calculated **g** values were in good agreement with experimental **g** values, but the calculated **A** values were systematically too small. Significantly, the trends in **g** and **A** with ligand substitution were reproduced very well by the calculations and were used to interpret the EPR data. The EPR parameters for the model complexes can be correlated to the V═O bond lengths.

I. Introduction

Electron paramagnetic resonance (EPR) spectroscopy has been used to investigate the electronic environment of paramagnetic transition metals in a variety of different systems.[1] In particular, transition metals, such as Cu^{2+} or V^{4+}, are widely studied by EPR spectroscopy because of their importance in biological and catalytic systems.[2−4] The EPR parameters, such as the electronic **g** tensor, and the hyperfine coupling constant or **A** tensor, depend on the coordination of the transition metal ion and on the properties of the ligands.[2,3,5] The parallel components of the **g** and **A** tensors ($\mathbf{g}_{||}$ and $\mathbf{A}_{||}$) are most sensitive to changes in geometry and ligand binding and can therefore be used to interpret experimental EPR data. In fact, for Cu^{2+} and VO^{2+} systems,[2,6] $\mathbf{g}_{||}$ and $\mathbf{A}_{||}$ of model complexes, are empirically correlated with respect to ligand identity and, in the case of Cu^{2+}, the charge of the complex. This empirical relationship between $\mathbf{g}_{||}$ and $\mathbf{A}_{||}$ has been used to identify coordinating groups in proteins and zeolites that contain copper or vanadium centers.[2,3,7−10] So far, these empirical relationships between $\mathbf{g}_{||}$ and $\mathbf{A}_{||}$ have been qualitatively understood in the context of ligand field theory.[11−13] To understand the correlation of $\mathbf{g}_{||}$ and $\mathbf{A}_{||}$ quantitatively, electronic structure methods for the calculation of **g** and **A** tensors are necessary.

Recent advances in computational chemistry have lead to the development of new methods for the calculation of electronic **g** and **A** tensors. Several groups have reported computational methods based on density functional theory (DFT) for calculating **g** tensors for transition metals.[14−18] Schreckenbach and Ziegler reported the implementation of a DFT method for the calculation of the **g** tensor.[17] Schreckenbach's method is based on the use of gauge-including atomic orbitals (GIAO) and second-order perturbation theory in which spin−orbit coupling is included to first order.[17] The treatment of spin−orbit coupling is very important to the calculation of **g** tensors because it is the primary interaction that shifts the g-values away from the free electron **g** value, $\mathbf{g}_e$, for transition metal systems.[18] Malkina and co-workers recently reported the use of another method for the calculation of EPR **g** tensors based on the deMon code.[14] In their method, the goal was to develop an accurate and efficient treatment of two-electron spin−orbit terms.[14] In the approach of van Lenthe, the spinor of the unpaired electron obtained from a DFT calculation is used to calculate the **g** tensor for a Kramer's doublet open shell molecule. Spin−orbit coupling is included variationally using the zeroth-order regular approximation (ZORA) to the Dirac equation.[18] A similar method for calculating **A** tensors was also developed.[19] The methods of van Lenthe[18,19] were recently included in the Amsterdam density functional (ADF) program[20−22] which is commercially available.

The DFT methods for calculating **g** and **A** tensors are all relatively new and have not yet been applied to a large number of systems. Schreckenbach's method for **g** tensor calculations has been successfully applied to d^1 transition metal complexes and metal porphyrins.[15,16] Similarly, Malkina and co-workers assessed their methods for **g** tensor calculations by applying

* To whom correspondence should be addressed. Fax: 319-335-1279. E-mail: sarah-larsen@uiowa.edu.

[†] Current address: Department of Chemical Physics, Weizmann Institute of Science, Rehovot 76100, Israel.

10.1021/jp010623e CCC: $20.00
Published on Web 04/05/2001

TABLE 1: ICP Results for VO^{2+}-Exchanged Zeolite Samples

zeolite sample	source	exchanged with:	Si/Al	exchange level[a] (%)	wt %
VO^{2+}-ZSM5-16-1	Zeolyst Corp.	$VOSO_4$	16	1	0.03
VO^{2+}-ZSM5-16-38	Zeolyst Corp.	$VOSO_4$	16	38	0.87
VO^{2+}-mordenite-5-11	Zeolyst Corp.	$VOSO_4$	5	11	0.65
VO^{2+}-Beta-13-17	Zeolyst Corp.	$VOSO_4$	13	17	0.46
VO^{2+}-Y-2-7	Aldrich	$VOSO_4$	2	7	0.77

[a] Exchange level = 2 × V/Al × 100%.

them to many different paramagnetic molecules, including aromatic radicals and transition metal complexes.[14] Munzarova and Kaupp reported a study of the validity of DFT methods for the calculation of **A** tensors for transition metal complexes.[23] They found that with gradient corrected functionals and hybrid functionals, **A** tensors could be calculated to within ~10−15% of the experimental values for many of the systems.[23] However, there are no reports of application of DFT methods in which the objective is to calculate **g** *and* **A** tensors in order to reproduce empirical correlations between **g** and **A** that are observed experimentally for transition metals, such as Cu^{2+} and VO^{2+}.[2,3,6]

In this study, experimental and theoretical EPR methods were combined to investigate the local electronic environment of VO^{2+} in VO^{2+}-exchanged zeolites. A series of VO^{2+}-exchanged zeolites (ZSM5, mordenite, Beta, and Y) were prepared by a standard aqueous ion exchange procedure. EPR spectra of the samples were obtained before and after dehydration and in the presence of ammonia. The role of the zeolite host in influencing the structural properties and the local electronic environment of VO^{2+} ions in the presence of reactant molecules was examined. Binding of ammonia to the VO^{2+} center in VO^{2+}-exchanged zeolites was monitored by analysis of the EPR spectrum. Trends in the EPR parameters obtained from VO^{2+}-exchanged zeolites with water versus ammonia ligands were identified. The methods of van Lenthe[18,19] as implemented in the ADF program[20−22] were used to calculate **g** and **A** tensors for VO^{2+} model complexes in order to assess whether the theoretical results would reproduce the empirical trends of the experimental EPR parameters. If successful, these theoretical methods could be used to interpret the EPR spectra of VO^{2+} complexes in zeolites and in many other systems. In particular, there is a great deal of interest in using EPR methods to investigate ligand binding in biological systems containing vanadyl ions.[3,6,24−34]

II. Experimental Section

Sample Preparation. The zeolites were purchased from commercial vendors: NaZSM5 (Zeolyst), HZSM5 (PQ Corporations), NH_4^+-Beta (Zeolyst), NaY (Aldrich), and Na-mordenite (Zeolyst). VO^{2+}-exchanged zeolites Y, mordenite, Beta, and ZSM5 were prepared using dilute solutions of vanadyl sulfate. The parent zeolite (~5.0 g) was added to 200 mL of 0.05 M aqueous vanadyl sulfate (pH~2.8) and stirred overnight at room temperature. The exchanged zeolite samples were then filtered and washed with 1.0 L of deionized water and dried overnight in an oven at 330 K. VO^{2+}-ZSM5 was prepared with two different vanadium exchange levels. To achieve the higher exchange level, the ZSM5 sample was exchanged twice.

Exchanged samples were characterized by ICP-AES (inductively coupled plasma atomic emission spectroscopy) using Perkin-Elmer Plasma 400 for elemental analysis. All of the samples were analyzed to determine the Si/Al ratios and the vanadium loading of the samples. The form of sample identification that will be used throughout this paper is *zeolite-Si/Al ratio-exchange level (%)* (i.e., VO^{2+}-ZSM5-14-24 has a Si/Al = 14 and a vanadium exchange level of 24%). The exchange level was calculated by taking the V/Al ratio from ICP results and multiplying by two to account for the theoretical exchange based on the charge compensation of one VO^{2+} for every two Al atoms (2 × V/Al × 100% = % V exchange). In other words, 100% exchange is obtained when the V/Al = 0.5 and the net negative charge of −1 introduced by substitution of an aluminum atom for a silicon atom in the zeolite framework is charge compensated by 0.5 VO^{2+}. The elemental analysis results for all of the samples used in this study are reported in Table 1.

Fresh or air exposed samples are referred to as *hydrated*. The dehydration procedure was performed on a vacuum rack using standard quartz EPR tubes with high vacuum valves attached. Pretreatment consisted of evacuation of the zeolite sample (~60 mg) for 1 h and subsequent ramping to 573 K over 1 h followed by holding at 573 K for 1 h under vacuum. Samples prepared using this pretreatment procedure are referred to as *dehydrated*.

Gas Adsorption. Prior to ammonia adsorption, the vanadium-exchanged zeolite samples were evacuated on a vacuum rack. Ammonia was introduced onto the samples by exposing each sample to ammonia gas (Matheson) for 30 min at room temperature to an equilibrium pressure of ~150 Torr. The samples were then evacuated for 5 min and sealed in an EPR tube fitted with a high vacuum valve.

Experimental Apparatus. CW EPR (continuous wave EPR) spectra were acquired using a Bruker EMX61 EPR spectrometer equipped with a PC for spectrometer control and data acquisition. A Bruker ER41111 Variable Temperature Unit with a temperature range of 110−673 K was used to heat and cool the sample. Typical EPR spectral parameters were X-band frequency = 9.43 GHz, modulation amplitude = 0.5 G, and modulation frequency = 100 kHz. The microwave frequency was measured using a frequency counter. DPPH was used to calibrate the magnetic field.

Least-Squares Fitting Program. The fitting program previously used for fitting copper EPR spectra was modified for the vanadium system ($S = {}^1/_2$; $I = {}^7/_2$).[8,10] This program is based on the method of Toy et al. [35] combined with a simplex least-squares fitting routine.[36] The method of Alderman et al. was used for the spherical average.[37] Axial symmetry and coincident **g** and **A** (^{51}V) tensors were assumed. Fit parameters included $\mathbf{A}_{\parallel}$, $\mathbf{g}_{\parallel}$, $\mathbf{A}_{\perp}$, $\mathbf{g}_{\perp}$. and a Gaussian broadening factor. The Gaussian broadening factor is defined as the full width at half-height of the Gaussian line.

Theoretical Methods. Geometry optimizations of six vanadyl model complexes, $VO(H_2O)_4^{2+}$, $VO(H_2O)_5^{2+}$, cis and trans $VO(NH_3)_2(H_2O)_2^{2+}$, $VO(NH_3)_4^{2+}$, and $VO(NH_3)_4H_2O^{2+}$ were performed using the Amsterdam density functional (ADF) program package.[20−22] The program implements numerical integration in Cartesian space[38] and gradients for geometry optimizations are solved analytically.[39,40] The vanadyl complexes were optimized within the restrictions of their respective point groups. $VO(H_2O)_4^{2+}$ and $VO(NH_3)_4^{2+}$ were optimized with C_{4v} symmetry and $VO(H_2O)_5^{2+}$, *trans*-$VO(NH_3)_2(H_2O)_2^{2+}$, and VO-

$(NH_3)_4H_2O^{2+}$ were optimized with C_{2v} symmetry. *cis*-$VO(NH_3)_2(H_2O)_2^{2+}$ was optimized with C_s symmetry. $VO(H_2O)_4^{2+}$ was also optimized with C_{2v} symmetry so that the effect of the orientation of the water ligands on the EPR parameters could be assessed. Because of the symmetry restrictions, the optimized geometry does not necessarily represent a minimum on the respective potential energy surface for the gas phase molecule. In the gas phase, the lowest energy structure will maximize the hydrogen bonding between ligands whereas in condensed phase systems, the hydrogen bonding will most likely be with surrounding solvent molecules. The situation may be entirely different in the zeolitic environment. For consistency, the optimized structures obtained without including solvent or zeolite effects, but with symmetry constraints will be used throughout this paper. This will allow a systematic study of the impact of the structure of the complex and the identity of the ligands on the calculated EPR parameters.

The equations and methods for calculation of **g** tensors[41] and **A** tensors are due to van Lenthe et al.[42] The basis set designated *V* in the ADF program was used in geometry optimizations, **g** tensor calculations and **A** tensor calculations. Basis set *V* is a triple-ζ basis of Slater-type orbitals with two polarization functions for H−Ar. In general, all electron calculations were performed with no frozen cores on the atoms of the molecule.

Relativistic effects were included in all calculations using the zero order relativistic approximation (ZORA).[43−47] Two methods of including the relativistic effects were utilized. Scalar relativistic effects were employed for geometry optimizations and **A** tensor calculations. Spin−orbit relativistic effects were employed for **g** tensor calculations. The relativistic atomic potentials necessary for the relativistic calculations for each atom were calculated using the auxiliary program DIRAC, which is supplied with the ADF program package. The density functional for all calculations used the VWN[48] local density approximation and the generalized gradient approximation, with the exchange correction of Becke[49] and the correlation correction of Perdew.[50] Each molecule studied contained one unpaired electron; therefore, geometry optimizations and **A** tensor calculations were performed spin-unrestricted while restrictions due to the **g** tensor calculation method require these calculations to be performed spin-restricted.

III. Results

EPR Spectra of Hydrated Vanadium-Exchanged Zeolites. The EPR spectra of hydrated VO^{2+}-exchanged zeolites are presented in Figure 1A−E. Each sample was cooled to 115 K for EPR data acquisition. All of the EPR spectra in Figure 1A−E are qualitatively similar and are characteristic of rigid limit VO^{2+} systems (V^{4+},d^1).[3] The EPR spectra are dominated by the axial hyperfine interaction between the unpaired electron spin ($S = {}^1/_2$) and the ^{51}V nuclear spin ($I = {}^7/_2$, 99.8% natural abundance).

The EPR spectra in Figure 1 were fit using a modification of a least-squares minimization program described previously.[7−9] The fitted EPR spectra were subjected to uniform Gaussian broadening. A typical example of the agreement between the experimental EPR spectrum and the least-squares fit to the spectrum is shown in Figure 2 for hydrated VO^{2+}-ZSM5-16-1. The EPR parameters obtained from the least-squares fits to the EPR spectra in Figure 1 are reported in Table 2. In all cases, the agreement between the experimental and the fitted EPR spectrum was very good.

The **g** and **A** values do not vary much for the hydrated VO^{2+}-exchanged zeolites used in this study. VO^{2+}-Y-2-7 exhibits decreased $\mathbf{A}_{\|}$ and $\mathbf{A}_{\perp}$ values relative to the other zeolites and this difference is apparent in Figure 1C where it can be seen that the low field EPR features for VO^{2+}-Y-2-7 are shifted

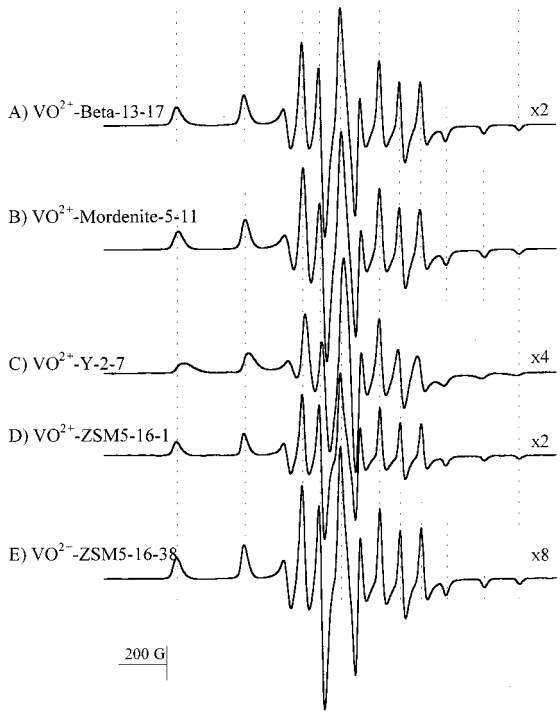

Figure 1. EPR spectra of hydrated VO^{2+}-exchanged zeolites, (A) VO^{2+}-Beta-13-17, (B) VO^{2+}-mordenite-5-11, (C) VO^{2+}-Y-2-7, (D) VO^{2+}-ZSM5-16-1, and (E) VO^{2+}-ZSM5-16-38. EPR spectra were acquired at 115 K and $\nu_{EPR} = 9.43$ GHz.

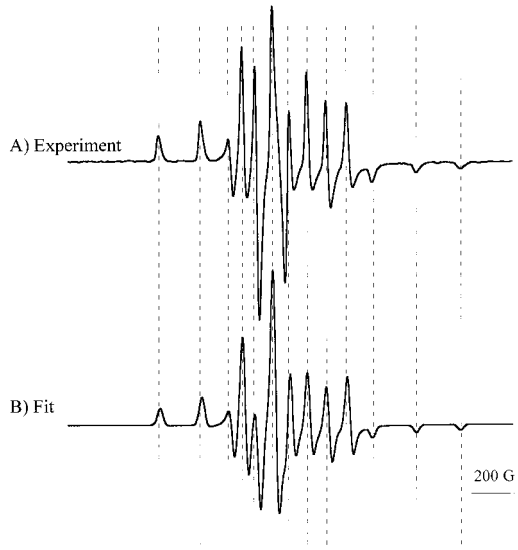

Figure 2. Comparison of the **(**A) experimental and (B) fitted EPR spectra of hydrated VO^{2+}-ZSM5-16-1. The experimental EPR spectrum was recorded at 115K and $\nu_{EPR} = 9.43$ GHz

TABLE 2: EPR Fitted Parameters[a] for Hydrated VO^{2+}-Exchanged Zeolites

sample	$\mathbf{A}_{\|}$ (MHz)	$\mathbf{A}_{\perp}$ (MHz)	$\mathbf{g}_{\|}$	$\mathbf{g}_{\perp}$	broadening (*G*)
VO^{2+}-ZSM5-16-1	549	218	1.933	1.997	31
VO^{2+}-ZSM5-16-38	550	218	1.933	1.997	32
VO^{2+}-mordenite-5-11	553	210	1.929	1.993	44
VO^{2+}-Beta-13-17	552	215	1.930	1.994	41
VO^{2+}-Y-2-7	536	193	1.931	1.990	47

[a] Estimated errors are ±0.001 for **g** and ±5 MHz for **A**.

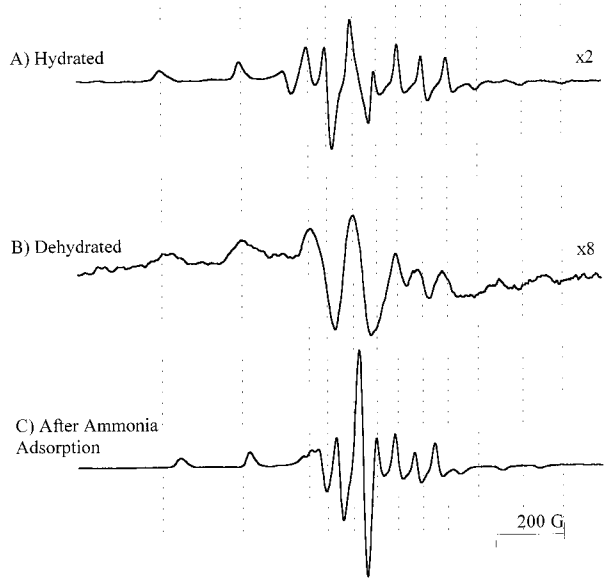

Figure 3. EPR spectra of VO^{2+}-ZSM5-16-1 (A) before pretreatment, (B) after pretreatment at 573 K under vacuum, and (C) after exposure of the hydrated sample to ammonia. EPR spectra were acquired at 115 K and $\nu_{EPR} = 9.43$ GHz.

TABLE 3: EPR Parameters for VO^{2+}-Exchanged Zeolites from the Literature

sample	$\mathbf{A}_{\|}$ (MHz)	$\mathbf{A}_{\perp}$ (MHz)	$\mathbf{g}_{\|}$	$\mathbf{g}_{\perp}$	source
$VO(H_2O)_5^{2+}$	534	210	1.936	1.982	54
$VO(H_2O)_5^{2+}$	547	212	1.933	1.978	3
VO^{2+}-ZSM5 (hydrated)	561	228	1.930	1.984	52
VO^{2+}-ZSM5 (dehydrated)	570	225	1.925	1.991	52
VO^{2+}-ZSM5 (hydrated)	566	218	1.923	1.972	53
VO^{2+}-Y (hydrated)	534	210	1.938	1.986	54
VO^{2+}-ZSM5 (hydrated)	549	231	1.941	1.983	51
VO^{2+}-ZSM5 (dehydrated)	546	227	1.925	1.987	51
VO^{2+}-ZSM5 (ammonia adsorbed)	494	193	1.955	1.984	51

relative to the other zeolites. The broadening of this EPR spectrum is also the largest compared to the others in Figure 1 and Table 2.

Some of the published experimental EPR parameters for VO^{2+}-exchanged zeolites and the model complex, $VO(H_2O)_5^{2+}$, are listed in Table 3. Most of the literature data available for VO^{2+}-exchanged zeolites is for VO^{2+}-ZSM5 (hydrated, dehydrated and with adsorbed NH_3)[51−53] and for VO^{2+}-Y (hydrated).[54] The EPR parameters for VO^{2+}-ZSM5 and VO^{2+}-Y from our work (Table 2) and the work (Table 3) of others are very consistent. In addition, the agreement between the EPR parameters for hydrated VO^{2+}-exchanged zeolites (Tables 2 and 3) and for the model complex, $VO(H_2O)_5^{2+}$, from the literature (Table 3) is quite good. For example, the $\mathbf{A}_{\|}$ ($\mathbf{g}_{\|}$) values for the VO^{2+}-exchanged zeolites in this study ranged from 536 MHz (1.931) for VO^{2+}-Y-2-7 to 553 MHz (1.929) for VO^{2+}-mordenite compared to $\mathbf{A}_{\|}$ ($\mathbf{g}_{\|}$) of 534 MHz (1.936) for the model complex, $VO^{2+}(H_2O)_5$.

EPR Spectra of Vanadium-Exchanged Zeolites After Dehydration or Adsorption of Ammonia. Figure 3 illustrates the changes in the EPR spectrum that occur as a result of dehydration or adsorption of ammonia. The EPR spectra of VO^{2+}-ZSM5-16-1 before and after dehydration under vacuum and after exposure of the hydrated sample to ammonia, are shown in Figure 3A−C, respectively. The EPR spectrum of dehydrated VO^{2+}-ZSM5-16-1 is substantially broader and the spectral features are shifted slightly relative to the EPR spectrum

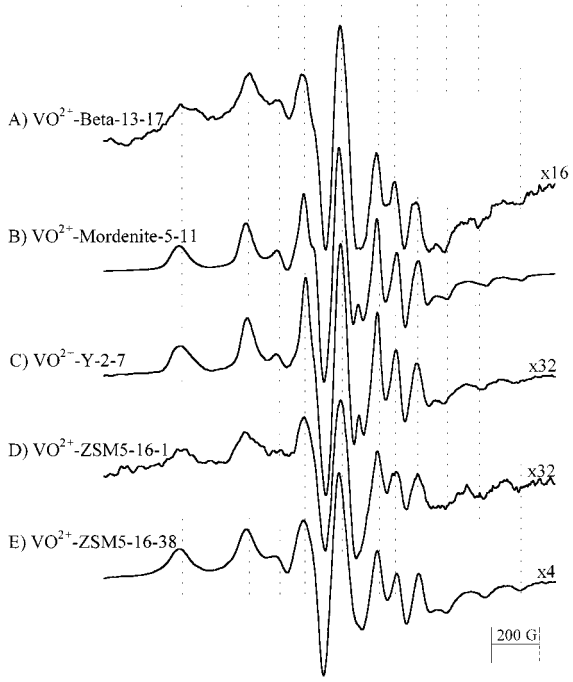

Figure 4. EPR spectra of VO^{2+}-exchanged zeolites after pretreatment under vacuum at 573 K, (A) VO^{2+}-Beta-13-17, (B) VO^{2+}-mordenite-5-11, (C) VO^{2+}-Y-2-7, (D) VO^{2+}-ZSM5-16-1, and (E) VO^{2+}-ZSM5-16-38. EPR spectra were acquired at 115 K and $\nu_{EPR} = 9.43$ GHz.

TABLE 4: EPR Fitted Parameters[a] for Dehydrated VO^{2+}-Exchanged Zeolites[a]

sample	$\mathbf{A}_{\|}$ (MHz)	$\mathbf{A}_{\perp}$ (MHz)	$\mathbf{g}_{\|}$	$\mathbf{g}_{\perp}$	broadening (*G*)
VO^{2+}-ZSM5-16-38	542	209	1.925	1.996	89
VO^{2+}-mordenite-5-11	551	205	1.922	1.996	70
VO^{2+}-Y-2-7	539	280	1.930	1.977	89

[a] Estimated errors are ±0.002 for **g** and ±15 MHz for **A**.

of hydrated VO^{2+}-ZSM5-16-1. For comparison, the EPR spectrum of hydrated VO^{2+}-ZSM5-16-1 after adsorption of ammonia is shown in Figure 3C. In this case, the EPR spectral features shift significantly after the adsorption of ammonia relative to the EPR features for hydrated VO^{2+}-ZSM5-16-1 indicating that ammonia binds to the VO^{2+} center.

The EPR spectra of the dehydrated VO^{2+}-exchanged zeolites, (A) VO^{2+}-Beta-13-17, (B) VO^{2+}-mordenite-5-11, (C) VO^{2+}-Y-2-7, (D) VO^{2+}-ZSM5-16-1, and (E) VO^{2+}-ZSM5-16-38, are shown in Figure 4A−E. The EPR parameters for the spectra in Figure 4B,C,E are listed in Table 4. The EPR parameters for VO^{2+}-Beta-13-17 (Figure 4A) and VO^{2+}-ZSM5-16-1 (Figure 4D) are not listed in Table 4 because the EPR parameters were determined by spectral simulation rather than fitting due to the low signal-to-noise ratio of the spectra. The EPR parameters determined from spectral simulation for dehydrated VO^{2+}-Beta-13-17 and VO^{2+}-ZSM5-16-1 agree qualitatively with the parameters for VO^{2+}-ZSM5-16-38. The EPR spectra of the dehydrated zeolites are all substantially broadened relative to the hydrated VO^{2+}-exchanged zeolites. The Gaussian broadening factors for the dehydrated VO^{2+}-exchanged zeolites are approximately twice as large as the Gaussian broadening factors for the hydrated VO^{2+}-exchanged zeolites. After the samples are dehydrated, the $\mathbf{A}_{\|}$ values change by ∼1−2% relative to the hydrated zeolites and the **g** values decrease.

The EPR spectra obtained after adsorption of ammonia on the VO^{2+}-exchanged zeolites are shown in Figure 5. The EPR parameters obtained from the least-squares fit to the data in

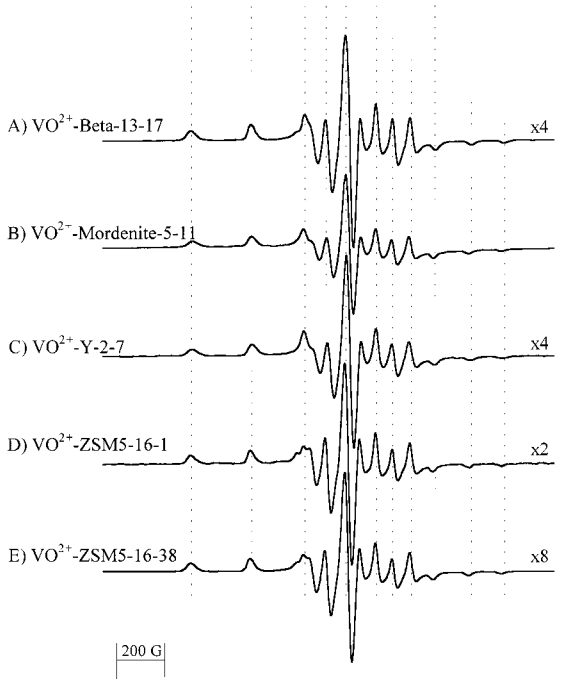

Figure 5. EPR spectra of hydrated VO^{2+}-exchanged zeolites after adsorption of NH_3, (A) VO^{2+}-Beta-13-17, (B) VO^{2+}-mordenite-5-11, (C) VO^{2+}-Y-2-7, (D) VO^{2+}-ZSM5-16-1, and (E) VO^{2+}-ZSM5-16-38. EPR spectra were acquired at 115 K and $\nu_{EPR} = 9.43$ GHz.

TABLE 5: EPR Fitted Parameters[a] for VO^{2+}-Exchanged Zeolites after Ammonia Adsorption[a]

sample	$\mathbf{A}_{\|}$ (MHz)	$\mathbf{A}_{\perp}$ (MHz)	$\mathbf{g}_{\|}$	$\mathbf{g}_{\perp}$	broadening (*G*)
VO^{2+}-ZSM5-16-1	495	175	1.942	1.990	33
VO^{2+}-ZSM5-16-38	503	175	1.942	1.989	35
VO^{2+}-mordenite-5-11	493	168	1.938	1.987	40
VO^{2+}-Beta-13-17	502	172	1.938	1.987	35
VO^{2+}-Y-2-7	491	166	1.941	1.986	39

[a] Estimated errors are ±0.001 for **g** and ±5 MHz for **A**.

Figure 5 are given in Table 5. $\mathbf{A}_{\|}$ decreases and $\mathbf{g}_{\|}$ increases relative to the EPR parameters of hydrated VO^{2+}-exchanged zeolites when ammonia is adsorbed. This suggests that ammonia binds to the vanadyl center. Similar EPR spectra (not shown) are observed when ammonia is adsorbed on dehydrated VO^{2+}-exchanged zeolites.

Geometry Optimization. The six model complexes, $VO(H_2O)_4^{2+}$, $VO(H_2O)_5^{2+}$, cis and trans $VO(NH_3)_2(H_2O)_2^{2+}$, $VO(NH_3)_4^{2+}$, and $VO(NH_3)_4H_2O^{2+}$ were geometry optimized. The resulting optimized structures are shown in Figure 6 and selected bond lengths and bond angles are listed in Table 6.

$VO(H_2O)_4^{2+}$ was restricted to C_{4v} and C_{2v} symmetry in two separate geometry optimizations. The resulting V═O bond length was 1.554 Å (C_{2v}, 1.555 Å) with equatorial V−O bond lengths of 2.071 Å (C_{2v}, 2.084, 2.040 Å). The energy of the $VO(H_2O)_4^{2+}$ optimized with C_{2v} symmetry was lower in energy than $VO(H_2O)_4^{2+}$ optimized with C_{4v} symmetry. $VO(H_2O)_5^{2+}$ was restricted to C_{2v} symmetry and the resulting V═O bond length was 1.568 Å with equatorial V−O bond lengths of 2.122 and 2.110 Å. The axial V−O bond length was 2.269 Å. The geometrical parameters obtained from the crystal structure for $VOSO_4 \cdot 5H_2O$[55] are listed in Table 6 for comparison with the optimized structures. The calculated V═O and V−O bond lengths for $VO(H_2O)_4^{2+}$ and $VO(H_2O)_5^{2+}$ deviate by 0.02−0.07 Å relative to the bond lengths from the crystal structure of $VOSO_4 \cdot 5H_2O$. The size of the deviations between the experimental and the calculated bond lengths are similar to those reported by Patchkovski and Ziegler for DFT geometry optimizations of d^1 MEX_4 transition metal complexes.[15]

$VO(NH_3)_4^{2+}$ was restricted to C_{4v} symmetry for the geometry optimization. The resulting V═O bond length was 1.562 Å with equatorial V−N bond lengths of 2.180 Å. $VO(NH_3)_4H_2O^{2+}$ was restricted to C_{2v} symmetry and the resulting V═O bond length was 1.575 Å with equatorial V−N bond lengths of 2.200 and 2.194 Å. The axial V−O bond length was 2.372 Å. *cis*- and *trans*-$VO(NH_3)_2(H_2O)_2^{2+}$ were geometry optimized with C_s and C_{2v} symmetry, respectively, and both have V═O bond lengths of 1.558 Å. The equatorial V−N and V−O bond lengths are 2.164 and 2.085 Å, respectively, for *trans*-$VO(NH_3)_2(H_2O)_2^{2+}$. The equatorial V−N and V−O bond lengths are 2.145 and 2.117 Å, respectively, for *cis*-$VO(NH_3)_2(H_2O)_2^{2+}$. The cis isomer is lower in energy than the trans isomer. Although there are no experimental structures available for comparison with the ammonia complexes, the expected trends in the bond lengths are reproduced by the calculations. The V−N bond lengths are longer than the V−O bond lengths reflecting weaker binding of the nitrogen ligands.[3]

Calculated EPR Parameters. Using the geometry optimized structures of the vanadyl model complexes, the **g** and **A** tensors were calculated using the ADF program and the methods of van Lenthe.[18,19] The resulting principal values of the **g** and **A**(**^{51}V**, **^{14}N**, and **^{1}H**) tensors are listed in Table 7. The **g** values calculated for $VO(H_2O)_5^{2+}$ ($\mathbf{g}_{\|} = 1.930$, $\mathbf{g}_{\perp} = 1.986$) deviate by 3−8 ppt (parts per thousand) from the experimental values for $VO(H_2O)_5^{2+}$ ($\mathbf{g}_{\|} = 1.933$, $\mathbf{g}_{\perp} = 1.978$[3] and $\mathbf{g}_{\|} = 1.936$, $\mathbf{g}_{\perp} = 1.982$[54]) which are listed in Table 3. The **g** values calculated for $VO(NH_3)_4^{2+}$ are $\mathbf{g}_{\|} = 1.957$, $\mathbf{g}_{\perp} = 1.985$. The systematic increase in $\mathbf{g}_{\|}$ with the introduction of nitrogen ligands is consistent with the empirical trend with ligand binding observed for vanadyl model complexes and will be discussed in more detail later.[3,6] The **A** values calculated for $VO(H_2O)_5^{2+}$ ($\mathbf{A}_{\|} = 408$; $\mathbf{A}_{\perp} = 148$ MHz) are systematically too low by approximately 25% when compared to the experimental values for $VO(H_2O)_5^{2+}$ ($\mathbf{A}_{\|} = 547$, $\mathbf{g}_{\perp} = 212$[3] and $\mathbf{g}_{\|} = 534$, $\mathbf{g}_{\perp} = 210$[54]) which are listed in Table 3. However, the empirical trend in $\mathbf{A}_{\|}$ values with ligand binding is reproduced by the calculations in that $\mathbf{A}_{\|}$ decreases systematically as ammonia ligands are added to the model complex. As might be qualitatively expected based on additivity relationships[3], the $\mathbf{g}_{\|}$ and $\mathbf{A}_{\|}$ values for *cis*- and *trans*-$VO(NH_3)_2(H_2O)_2^{2+}$ are between the $\mathbf{g}_{\|}$ and $\mathbf{A}_{\|}$ values for $VO(H_2O)_4^{2+}$ and $VO(NH_3)_4^{2+}$, respectively. However, the additivity relationships would predict that *cis*- and *trans*-$VO(NH_3)_2(H_2O)_2^{2+}$ would have the same **g** and **A** values which is not found in the calculations. Generally, the perpendicular components of the **g** and **A** values are less sensitive to changes in the VO^{2+} ligand environment than the parallel components.

The **g** and **A** values calculated for $VO(H_2O)_4^{2+}$ and $VO(H_2O)_5^{2+}$ are similar. This similarity in EPR parameters indicates that the influence of the axially coordinated ligand on the **g** and **A** values is small. Similarly, the **g** and **A** values for $VO(NH_3)_4^{2+}$ do not change much when the axial water ligand is added to form $VO(NH_3)_4H_2O^{2+}$.

The ligand hyperfine values for nitrogen, $\mathbf{A_N}$, and hydrogen, $\mathbf{A_H}$, are also calculated in the ADF program and are listed in Table 7. The ligand hyperfine interactions are not resolved in the EPR experiments described here, but the nitrogen and proton hyperfine coupling constants have been measured for various VO^{2+} systems using pulsed EPR and ENDOR (electron nuclear double resonance) experiments.[24,31,56−62]

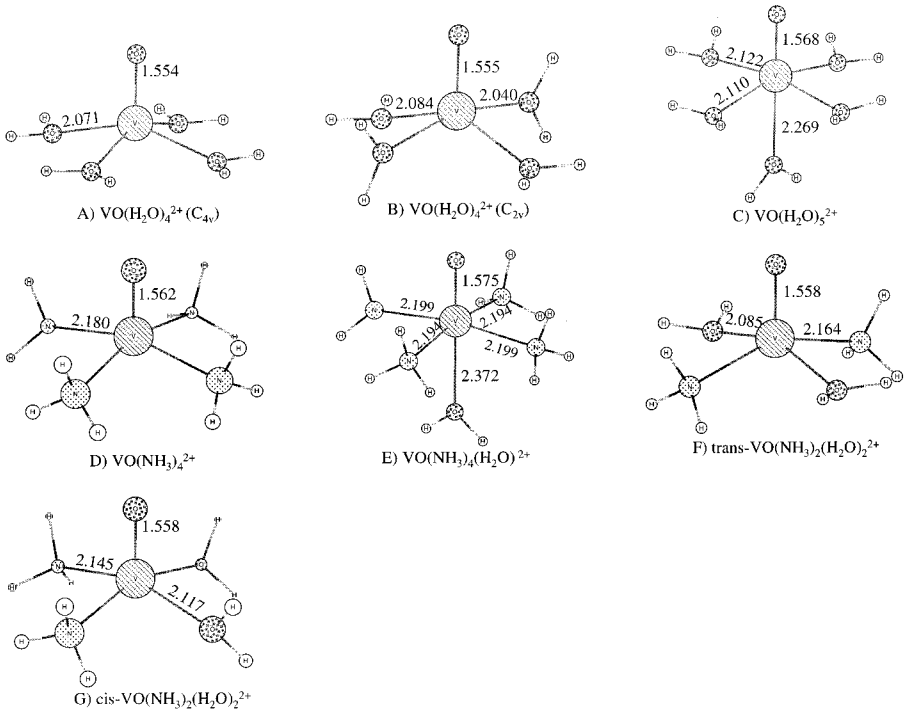

Figure 6. Optimized geometries for the model complexes: (A) $VO(H_2O)_4^{2+}(C_{4v})$, (B) $VO(H_2O)_4^{2+}(C_{2v})$, (C) $VO(H_2O)_5^{2+}$, (D) $VO(NH_3)_4^{2+}$, (E) $VO(NH_3)_4H+O^{2+}$, (F) *trans*-$VO(NH_3)_2(H_2O)_2^{2+}$, (G) *cis*-$VO(NH_3)_2(H_2O)_2^{2+}$. Bond lengths are given in angstroms.

TABLE 6: Selected Geometrical Parameters of VO^{2+} Model Compounds and Comparison with Experimental Values

		$R_{V=O}$, Å[a]		R_{V-L}, Å[b]		$\angle_{O=V-L}$[c]	
molecule	symmetry	calcd	exptl[d]	calcd	exptl[d]	calcd	exptl[d]
$VO(H_2O)_4^{2+}$	C_{4v}	1.554		2.071		105.4	
$VO(H_2O)_4^{2+}$	C_{2v}	1.555		2.084. 2.040		99.3, 109	
$VO(H_2O)_5^{2+}$	C_{2v}	1.568	1.591	2.110, 2.122 2.269 (axial)	2.035, 2.037 2.048, 1.983 (L = SO_4) 2.223 (axial)	99.5, 96.3	99.6, 97.9, 93.8, 100.7 (L=SO_4)
$VO(NH_3)_4^{2+}$	C_{4v}	1.562		2.180		100.85	
$VO(NH_3)_4H_2O^{2+}$	C_{2v}	1.575		2.199 (L=NH_3)2.194 (L = NH_3) 2.372 (L = H_2O, axial)		95.3, 95.5	
trans-$VO(NH_3)_2(H_2O)_2^{2+}$	C_{2v}	1.558		2.085 (L = H_2O) 2.164 (L = NH_3)		103.1 (L=H_2O) 107.4 (L=NH_3)	
cis-$VO(NH_3)_2(H_2O)_2^{2+}$	C_s	1.558		2.117 (L = H_2O) 2.145 (L = NH_3)		102.8 (L=H_2O) 101.1 (L=NH_3)	

[a] $R_{V=O}$ is the vanadyl bond distance [b] R_{V-L} is the bond distance between the vanadium ion and the ligand atoms. L refers to equatorial ligands unless labeled axial. [c] $\angle_{O=V-L}$ is the bond angle between the vanadium ion and the equatorial ligand atoms [d] From the crystal structure for $VOSO_4 \cdot 5H_2O$ from ref 55.

TABLE 7: EPR Parameters for VO^{2+} Model Complexes Calculated Using the ADF Program

molecule	symmetry	$\mathbf{g}_{11}$	$\mathbf{g}_{22}$	$\mathbf{g}_{33}$ ($\mathbf{g}_{\|}$)	$\lvert\mathbf{A}_{11}(\mathbf{A}_{\|})\rvert$[a]	$\lvert\mathbf{A}_{22}\rvert$[a]	$\lvert\mathbf{A}_{33}\rvert$[a]	$\lvert\mathbf{A}_N\rvert$[b]	$\lvert\mathbf{A}_H\rvert$[c]
$VO(H_2O)_4^{2+}$	C_{4v}	1.988	1.988	1.933	412	149	149		6.7, 6.9, 19.4
$VO(H_2O)_4^{2+}$	C_{2v}	1.985	1.979	1.924	409	142	141		8.4, 7.1, 4.7 7.1, 5.9, 6.7 5.1, 5.4, 18.0
$VO(H_2O)_5^{2+}$	C_{2v}	1.986	1.986	1.930	408	148	148		5.5, 5.8, 18.2 (eq[d]) 5.2, 5.5, 17.8 (eq[d]) 3.2, 3.1, 6.1 (axial)
$VO(NH_3)_4^{2+}$	C_{4v}	1.985	1.985	1.957	350	85	85	6.2, 5.9, 5.7	
$VO(NH_3)_4H_2O^{2+}$	C_{2v}	1.983	1.982	1.956	345	83	82	6.2, 5.9, 5.7 6.2, 5.9, 5.6	2.9, 2.8, 5.4(axial)
trans-$VO(NH_3)_2(H_2O)_2^{2+}$	C_{2v}	1.988	1.985	1.945	372	115	109	6.1, 5.9, 5.5	6.5, 6.8, 19.4
cis-$VO(NH_3)_2(H2O)_2^{2+}$	C_s	1.981	1.981	1.939	372	107	100	6.2, 5.9, 5.7 6.2, 5.9, 5.6	5.7, 4.9, 7.3 1.6, 0.9, 10.4

[a] Principal values ($\mathbf{A}_{11}$, $\mathbf{A}_{22}$, $\mathbf{A}_{33}$) of the vanadium (^{51}V) hyperfine tensor. The **A** values are reported in MHz. [b] Principal values ($\mathbf{A}_{11}$, $\mathbf{A}_{22}$, $\mathbf{A}_{33}$) of the nitrogen (^{14}N) hyperfine tensor. The **A** values are reported in MHz. [c] Principal values ($\mathbf{A}_{11}$, $\mathbf{A}_{22}$, $\mathbf{A}_{33}$) of the hydrogen (^{1}H) hyperfine tensor for water ligands. The **A** values are reported in MHz. [d] eq = equatorial.

IV. Discussion

The Effect of the Zeolite Host on the EPR Spectra of VO^{2+}-Exchanged Zeolites. The EPR spectra of hydrated VO^{2+}-exchanged zeolites, ZSM5, Beta, mordenite and Y, exhibited similar spectral features as shown in Figure 1. The EPR parameters, $\mathbf{g}_{\|}$ and $\mathbf{A}_{\|}$, listed in Tables 2, 4, and 5 are plotted in

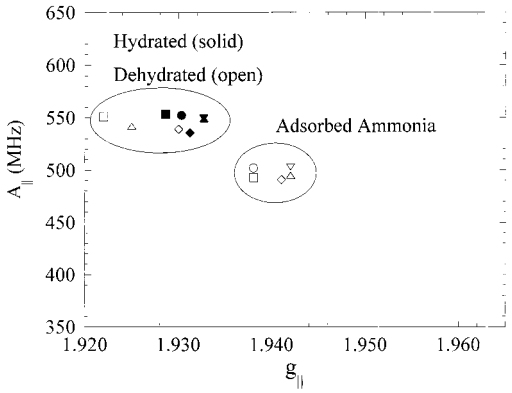

Figure 7. Correlation plot of $\mathbf{g}_{||}$ and $\mathbf{A}_{||}$ showing EPR parameters of hydrated (filled symbols) and dehydrated (open symbols, top ellipse) VO^{2+}-exchanged zeolites and VO^{2+}-exchanged zeolites after adsorption of ammonia (open symbols, lower right group). The following symbols (filled and open) were used to represent the different zeolites: VO^{2+}-Beta-13-17 (●), VO^{2+}-mordenite-5-11(■), VO^{2+}-Y-2-7 (◆), VO^{2+}-ZSM5-16-1(▲), and VO^{2+}-ZSM5-16-38 (▼).

Figure 7 so that the effect of the parent zeolite on the EPR parameters can be readily evaluated. The experimental EPR parameters for the hydrated VO^{2+}-exchanged zeolites are represented by the filled symbols and are located in the top ellipse in the graph shown in Figure 7. The EPR parameters for the hydrated VO^{2+}-exchanged zeolites are close to the EPR values reported for the $VO^{2+}(H_2O)_5$ complex.[54] The interpretation is that VO^{2+} coordinates five water molecules in the zeolite channels and that the water molecules in the first coordination sphere of the VO^{2+} complex, $VO(H_2O)_5^{2+}$, prevent the VO^{2+} ion from interacting with the zeolite framework. Therefore, the local electronic environment of $VO(H_2O)_5^{2+}$ in the different zeolites is not affected by the different structures and different Si/Al of the parent zeolites. This result agrees with our earlier work on copper-exchanged zeolites in which similar Cu^{2+} EPR spectra were observed for hydrated samples, independent of the identity and Si/Al of the parent zeolite.[8]

After dehydration, the $\mathbf{g}_{||}$ values decrease relative to the $\mathbf{g}_{||}$ values of the hydrated VO^{2+}-exchanged zeolites. The EPR parameters are plotted in Figure 7 as the open symbols in the top ellipse. This small change in EPR parameters can be interpreted as indicating that the local environment of the VO^{2+} ion changes, probably as a result of losing water ligands and coordinating to the zeolite lattice oxygens.[5,54] Petras and Witcherlova suggested that these changes in the EPR parameters indicated that the V═O bond is strengthened and that the in-plane V−O bonds are weakened relative to the hydrated VO^{2+} complex.[51] One possible explanation for the increase in broadening is increased site heterogeneity in the VO^{2+}-exchanged zeolites after dehydration. This would suggest that VO^{2+} binds to different sites in the zeolite causing the EPR signal to broaden due to the presence of many slightly different EPR signals. The observed increase in broadening of the dehydrated vs the hydrated VO^{2+}-exchanged zeolites has been observed previously by Prakash and Kevan.[5]

The Effect of Ammonia Adsorption on the EPR Parameters of VO^{2+}-Exchanged Zeolites. After adsorption of ammonia, the EPR parameters for the VO^{2+}-exchanged zeolites systematically change relative to the hydrated and dehydrated VO^{2+}-exchanged zeolites. $\mathbf{A}_{||}$ decreases and $\mathbf{g}_{||}$ increases relative to $\mathbf{A}_{||}$ and $\mathbf{g}_{||}$ for the hydrated and dehydrated zeolites indicating that ammonia binds to the VO^{2+} ion. The same effect is observed independent of the parent zeolite as can be seen from the grouping of the EPR parameters for VO^{2+}-exchanged zeolites with adsorbed ammonia in the lower ellipse in Figure 7. Petras and Witcherlova observed similar changes in the EPR parameters after ammonia adsorption on dehydrated VO^{2+}-HZSM5.[51] They interpreted this change in EPR parameters as indicating a strengthening of the in-plane V−O bonds and a weakening of the V═O bond relative to the dehydrated VO^{2+}-exchanged zeolite.[51]

The EPR spectra do not provide information about the number of ammonia atoms that bind to the VO^{2+} center because the inhomogeneous broadening of the EPR spectrum is larger than the line width of typical nitrogen hyperfine interactions.[3,63] For VO^{2+} complexes, the experimental isotropic hyperfine coupling constant for a simple amine coordinated to the oxovanadium bond ranges from ∼3−6 MHz for cis coordination to ∼0 for trans coordination relative to the V═O bond.[24,57,58,62,63] Pulsed EPR and ENDOR spectroscopy have been used to determine the number and coordination of nitrogen ligands in VO^{2+} complexes.[24,57,58,62,63] In an ESEEM (electron spin−echo envelope modulation) spectroscopy study, Prakash and Kevan determined that ammonia was bound to VO^{2+} in VS-1 cis to the oxovanadium bond.[5]

Interpretation of the EPR Spectra of VO^{2+}-Exchanged Zeolites Using Computational Results. A correlation between $\mathbf{g}_{||}$ and $\mathbf{A}_{||}$ was previously observed for model VO^{2+} complexes containing oxygen, nitrogen, and sulfur ligands.[3,6] The EPR parameters, $\mathbf{g}_{||}$ and $\mathbf{A}_{||}$, for vanadyl model complexes containing similar ligands (oxygen, nitrogen or sulfur) can be grouped together such that the values of $\mathbf{g}_{||}$ and $\mathbf{A}_{||}$ can be used as indicators of ligand binding. To understand the physical basis for the empirical correlation between $\mathbf{g}_{||}$ and $\mathbf{A}_{||}$ for some of these model complexes, EPR parameters for VO^{2+} model complexes were calculated using the ADF program. The calculated **g** values for the model complexes $VO(H_2O)_4^{2+}(C_{4v})$ and $VO(H_2O)_5^{2+}$ were very accurate and were in good agreement (deviations of ∼ 3 ppt) with the experimental values. However, the calculated **A (^{51}V)** values for $VO(H_2O)_4^{2+}$ and $VO(H_2O)_5^{2+}$ were systematically too small by approximately 25%.

Knight and co-workers have reported ab initio calculations of the EPR parameters for simple vanadium radicals (VO_2, VO_3), but these methods are still very time-consuming and expensive for larger molecules.[64] Although DFT methods are much less expensive for calculations on transition metal systems, there are only a few examples in the literature of DFT calculations of hyperfine coupling constants for transition metal complexes containing vanadium.[23,65,66] Munzarova and Kaupp presented the first systematic study in which the hyperfine coupling constants of 21 transition metal complexes were calculated using DFT methods.[23] They found that, for the best cases, the isotropic hyperfine coupling constants could be determined to within 10−15%, but that in other cases the differences between the experimental and calculated hyperfine coupling constants were even greater.[23] They attributed the difficulties in calculating the hyperfine coupling constants for transition metal systems to spin polarization and spin contamination effects.[23] In a subsequent paper, Munzarova and Kaupp investigated spin polarization effects in detail.[65] They concluded that improved functionals that give increased spin polarization without increasing the spin contamination would need to be developed in order to improve the agreement between the calculated and experimental hyperfine coupling constants.[23]

With these results in mind, it is not surprising that the calculated hyperfine coupling constants for the vanadyl ($3d^1$) model complexes in this study are systematically too low by

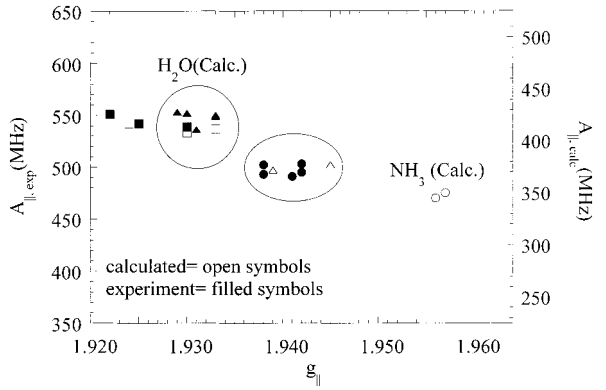

Figure 8. Correlation plot of $\mathbf{g}_{\|}$ and $\mathbf{A}_{\|}$ showing experimental EPR parameters of (▲) hydrated and (■) dehydrated VO^{2+}-exchanged zeolites and VO^{2+}-exchanged zeolites after (●) adsorption of ammonia. The calculated EPR parameters for vanadyl model complexes are graphed using open symbols: (□) for $VO(H_2O)_4^{2+}$ and $VO(H_2O)_5^{2+}$ and (○) for $VO(NH_3)_4^{2+}$ and $VO(NH_3)_4H_2O^{2+}$ and (△) for *cis*- and *trans*-$VO(NH_3)_2(H_2O)_2^{2+}$.

25%. This deviation can be attributed to spin polarization and spin contamination effects, which have been shown to be important for transition metals particularly when the unpaired electron is in a d orbital. The spin polarization and contamination effects are not treated adequately with the currently available functionals. However, since the vanadium model complexes in this study are expected to have similar spin polarizations and contaminations, the deviation in calculated **A** values is systematic and leads to calculated hyperfine coupling constants that are all approximately 25% too low. Therefore, trends in experimental hyperfine coupling constants can be reproduced and interpreted qualitatively.

The experimental and calculated EPR parameters, $\mathbf{g}_{\|}$ and $\mathbf{A}_{\|}$, are plotted in Figure 8 for the VO^{2+}-exchanged zeolites and for the VO^{2+} model complexes. The data are plotted on a double *y* axis to account for the systematic deviation of the $\mathbf{A}_{\|}$ values. The filled squares and filled triangles represent the experimental EPR parameters for the dehydrated and hydrated VO^{2+}-exchanged zeolites, respectively. The filled circles represent the experimental EPR parameters for the hydrated VO^{2+}-exchanged zeolites after adsorption of ammonia. The open symbols represent the calculated EPR parameters for the VO^{2+} model complexes. The open squares represent $VO(H_2O)_4^{2+}$ (C_{4v} and C_{2v}) and $VO(H_2O)_5^{2+}$ and the open circles represent $VO(NH_3)_4^{2+}$ and $VO(NH_3)_4(H_2O)^{2+}$. The open triangles represent *cis*- and *trans*-$VO(NH_3)_2(H_2O)_2^{2+}$.

The calculated EPR parameters for the model complexes $VO(H_2O)_5^{2+}$ and $VO(H_2O)_4^{2+}(C_{4v})$ complexes are qualitatively similar to the experimental EPR parameters for the hydrated VO^{2+}-exchanged zeolites as shown in Figure 8. Therefore, the vanadyl species present in hydrated VO^{2+}-exchanged zeolites (ZSM5, beta, mordenite and Y) is assigned to $VO(H_2O)_5^{2+}$ or $VO(H_2O)_4^{2+}$. Previously, based on the similarities in the EPR and ENDOR spectra of VO^{2+}-exchanged zeolites and $VO(H_2O)_5^{2+}$, several groups concluded that the species in hydrated VO^{2+}-ZSM5 and VO^{2+}-Y was $VO(H_2O)_5^{2+}$.[5,51,54,59,60,67]

The next question to address is how the orientation of the equatorial water ligands affects the EPR parameters. The $\mathbf{g}_{\|}$ value for $VO(H_2O)_4^{2+}(C_{2v})$ is decreased relative to the $\mathbf{g}_{\|}$ values for $VO(H_2O)_5^{2+}$ and $VO(H_2O)_4^{2+}(C_{4v})$ suggesting that the $\mathbf{g}_{\|}$ values are sensitive to the orientation of the water molecules in the equatorial plane (see Figure 6). Examination of the calculated proton hyperfine coupling constants for the water ligands in $VO(H_2O)_5^{2+}$ reveal two nearly equivalent protons from equatorial water molecules with coupling constants of 5.5, 5.8, 18.2 MHz and 5.2, 5.5, 17.8 MHz and protons from an axial water molecule with coupling constants of 3.2, 3.1 and 6.1 MHz. Experimental ^{1}H ENDOR results for $VO(H_2O)_5^{2+}$ are listed in Table 8.[59] The ENDOR results indicate that water molecules bound equatorial to V═O exhibit ^{1}H hyperfine coupling constants of 1, 1, and 17 MHz and water molecules bound axial to V═O exhibit ^{1}H hyperfine coupling constants of 3.3, 3.3, and 5.7 MHz.[59] While the quantitative agreement between the experimental and calculated proton hyperfine coupling constants is poor for the equatorial water molecules, the qualitative agreement is quite good, particularly when comparing the calculated $\mathbf{A_{33}}$ (17.8 and 18.2 MHz) for the equatorial water protons of $VO(H_2O)_5^{2+}$ with the experimental value of $\mathbf{A_z}$ (17 MHz) measured for $VO(H_2O)_5^{2+}$ by ENDOR.[59]

TABLE 8: Proton Hyperfine Coupling Constants for $VO(H_2O)_5^{2+}$ in Frozen Solution Measured by ENDOR Spectroscopy[59]

coordination of H_2O	$\lvert\mathbf{A}_x\rvert$ (MHz)	$\lvert\mathbf{A}_y\rvert$ (MHz)	$\lvert\mathbf{A}_z\rvert$ (MHz)	ref
equatorial	1.0	1.0	17	59
axial	3.3	3.3	5.7	59

The calculated proton hyperfine coupling constants for $VO(H_2O)_4^{2+}(C_{4v})$ are 6.7, 6.9, and 19.4 MHz. For $VO(H_2O)_4^{2+}(C_{2v})$, the protons for two of the water molecules are above and below the equatorial plane (ie the water molecule is rotated 90° relative to the equatorial plane, see Figure 6) while the protons of the other two water molecules are in the equatorial plane. The nearly equivalent calculated proton hyperfine coupling constants listed in Table 7 are 8.4, 7.1, 4.7 and 7.1, 5.9, 6.7 MHz for water molecules rotated 90° relative to the equatorial plane and 5.1, 5.4, 18.0 MHz for equatorial water molecules. Water molecules with the protons located in the equatorial plane (or nearly in the equatorial plane) have calculated proton hyperfine coupling constants with a distinctive $\mathbf{A_{33}}$ value of 17−18 MHz. Experimentally, this same distinctive proton hyperfine coupling constant of ∼17 MHz is observed for $VO(H_2O)_5^{2+}$ (in frozen solution) in ENDOR experiments.[59] The agreement between the experimental proton hyperfine coupling constants and the calculated proton hyperfine coupling constants for $VO(H_2O)_5^{2+}$ suggests that the observed ENDOR proton coupling constants are due to water molecules in $VO(H_2O)_5^{2+}$ that are oriented with the protons in or nearly in the equatorial plane. Single crystal ENDOR studies of $VO(H_2O)_5^{2+}$ in $Mg(NH_4)_2(SO_4)_26H_2O$ indicated that 2 equatorial water molecules were oriented in the equatorial plane and the other 2 equatorial water molecules were oriented perpendicular to the plane.[68] This suggests that the orientation of the water molecules is dependent on the solvation environment.

When ammonia is added to VO^{2+}-exchanged zeolites, $\mathbf{g}_{\|}$ increases and $\mathbf{A}_{\|}$ decreases. This same trend in $\mathbf{g}_{\|}$ and $\mathbf{A}_{\|}$ was observed in the calculated EPR parameters for the model complexes, $VO(NH_3)_4^{2+}$ and $VO(NH_3)_4H_2O^{2+}$ relative to the $VO(H_2O)_5^{2+}$ and $VO(H_2O)_4^{2+}$ model complexes. However, the calculated $\mathbf{g}_{\|}$ values for the model complexes were much higher than the experimental $\mathbf{g}_{\|}$ values for the VO^{2+}-exchanged zeolites with adsorbed ammonia. Better agreement between calculated and experimental EPR parameters for the VO^{2+}-exchanged zeolites with adsorbed ammonia was obtained by considering the mixed system, $VO(NH_3)_2(H_2O)_2^{2+}$ which has $\mathbf{g}_{\|}$ and $\mathbf{A}_{\|}$ values intermediate between $VO(H_2O)_4^{2+}$ and $VO(NH_3)_4^{2+}$. The cis- and trans structures of $VO(NH_3)_2(H_2O)_2^{2+}$ give somewhat different calculated EPR parameters, but both sets of parameters fall between the EPR parameters for $VO(H_2O)_4^{2+}$ and $VO(NH_3)_4^{2+}$ as shown in Figure 8.

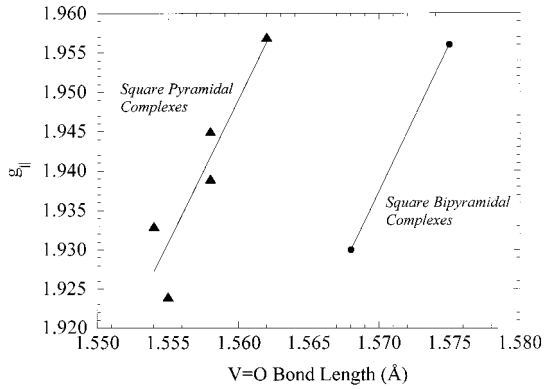

Figure 9. Dependence of the calculated $\mathbf{g}_{||}$ values on the V═O bond length (Å) for the square pyramidal ($VO(H_2O)_4^{2+}$, *cis*- and *trans*-$VO(NH_3)_2(H_2O)_2^{2+}$, $VO(NH_3)_4^{2+}$) and square bipyramidal complexes ($VO(H_2O)_5^{2+}$ and $VO(NH_3)_4H_2O^{2+}$).

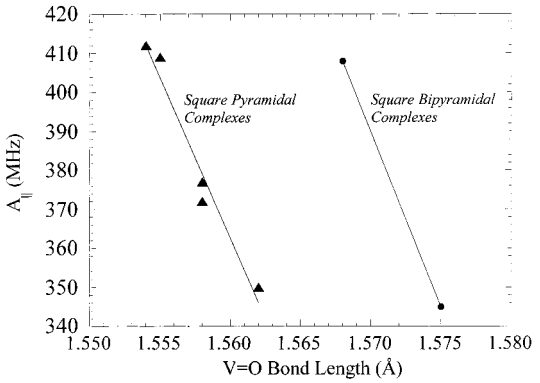

Figure 10. Dependence of the calculated $\mathbf{A}_{||}$ values on the V═O bond length (Å) for the square pyramidal ($VO(H_2O)_4^{2+}$, *cis*- and *trans*-$VO(NH_3)_2(H_2O)_2^{2+}$, $VO(NH_3)_4^{2+}$) and square bipyramidal complexes ($VO(H_2O)_5^{2+}$ and $VO(NH_3)_4H_2O^{2+}$).

On the basis of a comparison of the computational results for the various model complexes, the VO^{2+} complex present in the zeolite after exposure to ammonia is most likely *cis*- or *trans*-$VO(NH_3)_2(H_2O)_2^{2+}$ rather than $VO(NH_3)_4^{2+}$. This result makes sense since in the experiments, ammonia was adsorbed onto hydrated VO^{2+}-exchanged zeolites. Therefore, the ammonia must displace water ligands in the VO^{2+} complex. This result is further supported by the following characteristics of VO^{2+} systems with respect to binding of nitrogen ligands. Ethylenediamine must be present in a 1000:1 ligand to VO^{2+} ratio to compete with hydrolysis of VO^{2+} at pH = 7.[69] In general, weak binding of NH_2 groups to VO^{2+} is observed presumably because these ligands lack orbitals which can π-bond to d orbitals on vanadium.[3] The weak binding is reflected in longer V−N equatorial bond lengths as observed in the geometry optimized VO^{2+} model complexes.

The results shown in Figure 8 can be further interpreted to indicate that the $VO(NH_3)_2(H_2O)_2^{2+}$ species in the zeolite after exposure to ammonia is present as the cis isomer. Consistent with this assignment is the fact that the calculated energy for the cis isomer is lower than for the trans isomer. However, more computational work needs to be done to further evaluate the accuracy of the DFT methods for the calculation of **g** and **A** tensors of VO^{2+} model complexes before this assignment can be certain.

Correlation of Calculated EPR Parameters with the V═O Bond Length. These computational results demonstrate the potential of DFT calculations for the interpretation of EPR spectra of transition metal complexes. The calculated **g** values agree remarkably well with experimental values for the vanadyl model complexes considered in this study. The **A(^{51}V)** values are systematically too low by approximately 25%, but exhibit the same trends with ligand identity as the model complexes. Reproducing the empirical trend in $\mathbf{g}_{||}$ and $\mathbf{A}_{||}$ for VO^{2+} model complexes is the first step in applying DFT methods to the interpretation of EPR parameters. The next step for enhancing the interpretation of experimental EPR spectra is to use the computational results to elucidate the structure and bonding environment of VO^{2+}.

Selected computational results from Tables 6 and 7 are plotted in Figures 9 and 10. The relationship between the V═O bond length and $\mathbf{g}_{||}$ for all of the model complexes is plotted in Figure 9. There is a clear correlation between the V═O bond length and $\mathbf{g}_{||}$ for the model complexes of similar geometry. In other words, the square pyramidal and square bipyramidal model complexes, respectively, each show a clear dependence of $\mathbf{g}_{||}$ on the V═O bond length. For complexes with the same geometry, $\mathbf{g}_{||}$ increases as the V═O bond length increases. The relationship between the V═O bond length and $\mathbf{A}_{||}$ for all of the model complexes is plotted in Figure 10. Analogous to the results in Figure 9, there is a clear correlation between the V═O bond length and $\mathbf{A}_{||}$ for the model complexes of similar geometry. However, in this case, $\mathbf{A}_{||}$ decreases as the V═O bond length increases. Experimentally, for VO^{2+} model complexes, $\mathbf{g}_{||}$ decreases as $\mathbf{A}_{||}$ increases when changing the ligand from oxygen to nitrogen.

The results in Figures 9 and 10 show that for VO^{2+} complexes with the same geometry changes in the EPR parameters, $\mathbf{g}_{||}$ and $\mathbf{A}_{||}$, reflect changes in the V═O bond length. There are certainly other structural and bonding factors that impact the EPR parameters for VO^{2+} complexes. For example, the $\mathbf{g}_{||}$ values of $VO(H_2O)_4^{2+}$ (C_{4v}) and $VO(H_2O)_4^{2+}$ (C_{2v}) are quite different even though the V═O bond lengths only differ by 0.001 Å. Overall, the correlation of the V═O bond length is not as good for the $\mathbf{g}_{||}$ values compared to the $\mathbf{A}_{||}$ values, suggesting that other structural and electronic factors also impact the $\mathbf{g}_{||}$ values. Further work is under way with a more extensive group of model complexes to elucidate other structural factors that influence the EPR parameters.

Other structural effects on **g** and **A** should be investigated as well. For example, for VO^{2+} zeolites, the effect of structural perturbations, such as those imposed by the zeolite framework, on the geometries and EPR parameters of the model complexes will be investigated. Various cluster methods for introducing the zeolite framework into DFT calculations have been used for energy calculations.[70,71] In this way, VO^{2+} EPR signals may potentially be assigned to specific sites in the zeolite framework and specific bonding motifs may be elucidated.

Implications for Future Work. This is the first application of DFT methods in which an empirical correlation between the EPR parameters, $\mathbf{g}_{||}$ and $\mathbf{A}_{||}$, was reproduced for vanadyl model compounds. The accuracy of the **g**-values is quite good, but the **A** values are systematically too low. In a previous study by Munzarova and Kaupp, it was found that calculated **A** values deviated ∼10−15% from experimental values for transition metal complexes due to core−shell spin polarization and spin contamination effects.[23] Future work will focus on expanding the calculations to a larger range of VO^{2+} model complexes so that the relationship between electronic structure and g-values can be explored in more detail. The ADF calculations of EPR parameters have a great deal of potential for guiding the interpretation of the experimental EPR spectra for a wide variety of VO^{2+} complexes.

The extension of these DFT methods to other transition

metals, such as Cu^{2+}, which show similar empirical trends in EPR parameters, seems to be problematic. In the work of Malkina, the calculated **g** tensors for Cu^{2+} complexes deviated significantly from experimental results.[14] Similarly, our ADF calculations of EPR parameters for copper model complexes have shown significant deviations from the experimental values and have failed to predict the correct empirical trends in $\mathbf{g}_{||}$ and $\mathbf{A}_{||}$.[10] Others have noted similar difficulties with respect to calculations of EPR parameters for transition metal complexes using DFT methods and have attributed the discrepancies between experimental and theoretical results to deficiencies in gradient corrected functionals.[14−16,72] These transition metal systems will provide a good test for the next generation of DFT methods for the calculation of EPR parameters.

Another aspect of this work that will potentially have a large impact on the interpretation of experimental EPR, pulsed EPR, and ENDOR spectra is the calculation of ligand hyperfine tensors. Experimentally, these quantities are often measured by pulsed EPR techniques, such as ESEEM (electron spin−echo envelope modulation) or ENDOR.[24,57,58,60−62] In a study by Larsen and Singel, the nitrogen hyperfine interaction for ammonia adsorbed on silica supported vanadium oxide was measured to be ∼4.7 MHz using ESEEM spectroscopy.[61] The calculated nitrogen hyperfine coupling constants for the vanadyl model complexes (Table 7) with ammonia ligands investigated in the current study were ∼6 MHz. The calculated values are approximately 20% too high relative to the experimental value, which is approximately the same % as was found for ^{51}V hyperfine values in this study. Munzarova and Kaupp also considered ligand hyperfine in their work and determined that the agreement with experiment was reasonably good for some cases.[23] In addition, important structural information about the orientation of protons in VO^{2+} complexes may be obtained by calculating the proton hyperfine coupling constants for model complexes and comparing with experimental ENDOR results. Further work is needed to evaluate the usefulness of applying these DFT methods to the interpretation of ligand hyperfine coupling constants.

V. Conclusions

DFT calculations using the ADF code were utilized to predict the empirical relationship between $\mathbf{g}_{||}$ and $\mathbf{A}_{||}$ for VO^{2+} complexes. Using the computational results the experimental EPR spectra of VO^{2+}-exchanged zeolites were interpreted. The EPR spectra of the hydrated VO^{2+}-exchanged zeolites were all similar, independent of the parent zeolite. The EPR signal was attributed to a $VO(H_2O)_5^{2+}$ complex in the zeolite. After adsorption of ammonia, the experimental EPR spectrum systematically changed and $\mathbf{A}_{||}$ decreased and $\mathbf{g}_{||}$ increased relative to $\mathbf{A}_{||}$ and $\mathbf{g}_{||}$ of the hydrated zeolites.

EPR parameters were calculated for VO^{2+} model complexes using the ADF program. The calculated **g** values were very accurate, but the calculated **A** values were systematically too low. On the basis of the computational results, the VO^{2+} species present in the zeolite after exposure to ammonia was assigned to *cis*-$VO(NH_3)_2(H_2O)_2^{2+}$. Comparison of ENDOR data for $VO(H_2O)_5^{2+}$ with the calculated proton hyperfine coupling constants for $VO(H_2O)_5^{2+}$ show that the calculations can be used to determine the orientation of the equatorial water molecules. Calculated $\mathbf{g}_{||}$ and $\mathbf{A}_{||}$ values for the model complexes with the same geometry correlated with the V═O bond length.

Acknowledgment. S.L. gratefully acknowledges the support of NSF (CTS-99-73431). S.I. acknowledges support under an NSF REU grant (REU 9912191) at the University of Iowa. P.C. and S.L. acknowledge Professor Jan Jensen for helpful discussions and Sandy Baccam for data analysis.

Supporting Information Available: The optimized Cartesian coordinates for the model complexes, $VO(H_2O)_4^{2+}$ (C_{4v} and C_{2v}), $VO(H_2O)_5^{2+}$, $VO(NH_3)_4^{2+}$, $VO(NH_3)_4H_2O^{2+}$, *cis*- and *trans*-$VO(NH_3)_2(H_2O)_2^{2+}$, in Tables S1−S7. The material is available free of charge via the Internet at http://pubs.acs.org.

References and Notes

(1) Weil, J. A.; Bolton, J. R.; Wertz, J. E. *Electron Paramagnetic Resonance: Elementary Theory and Practical Applications*; John Wiley & Sons, Inc.: New York, 1994.
(2) Peisach, J.; Blumberg, W. E. *Arch. Biochem. Biophys.* **1974**, *165*, 691.
(3) Chasteen, N. D. In *Biological Magnetic Resonance*; Berliner, L. J., Reuben, J., Eds.; Plenum: New York, 1981; Vol. 3; p 53.
(4) Boas, J. F.; Pilbrow, J. R.; Smith, T. D. In *Biological Magnetic Resonance*; Berliner, L. J., Reuben, J., Eds.; Plenum Press: New York, 1978; Vol. 1; p 277.
(5) Prakash, A. M.; Kevan, L. *J. Phys. Chem. B* **2000**, *104*, 6860.
(6) Holyk, N. H. An EPR Study of Model Oxovanadium(IV) Complexes in Aqueous Solutions. MS Thesis, University of New Hampshire, 1979.
(7) Carl, P. J.; Larsen, S. C. *J. Catal.* **1999**, *182*, 208.
(8) Carl, P. J.; Larsen, S. C. *J. Phys. Chem. B* **2000**, *104*, 6568.
(9) Carl, P. J.; Baccam, S.; Larsen, S. C. *J. Phys. Chem. B.* **2000**, *104*, 8848.
(10) Carl, P. J. Characterization of Transition Metal Exchanged Zeolites by Electron Paramagnetic Resonance Spectroscopy. PhD Thesis, University of Iowa, 2000.
(11) Balhausen, C. J.; Gray, H. B. *Inorg. Chem.* **1962**, *1*, 111.
(12) Kivelson, D.; Lee, S.-K. *J. Chem. Phys.* **1964**, *41*, 1896.
(13) Smith, D. W. *J. Chem. Soc. A* **1970**, 3108.
(14) Malkina, O. L.; Vaara, J.; Schimmelpfennig, B.; Munzarova, M.; Malkin, V. G.; Kaupp, M. *J. Am. Chem. Soc.* **2000**, *122*, 9206.
(15) Patchkovskii, S.; Ziegler, T. *J. Chem. Phys.* **1999**, *111*, 5730.
(16) Patchkovskii, S.; Ziegler, T. *J. Am. Chem. Soc.* **2000**, *122*, 3506.
(17) Schreckenbach, G.; Ziegler, T. *J. Phys. Chem. A* **1997**, *101*, 3388.
(18) van Lenthe, E.; Wormer, P. E. S.; van der Avoird, A. *J. Chem. Phys.* **1997**, *107*, 2488.
(19) van Lenthe, E.; van der Avoird, A.; Wormer, P. E. S. *J. Chem. Phys.* **1998**, *108*, 4783.
(20) Baerends, E. J.; Ellis, D. E.; Ros, P. *Chem. Phys.* **1973**, *2*, 41.
(21) *Methods and Techniques in Computational Chemistry METECC-95*; Guerra, F. C., Visser, O., Snijders, J. G., te Velde, G., Baerends, E. J., Eds.; STEF: Cagliari, 1995; p 305.
(22) ADF http://tc.chem.v.nl/SCM. Department of Theoretical Chemistry, Vrije Universiteit: Amsterdam,, 1999.
(23) Munzarova, M.; Kaupp, M. *J. Phys. Chem. A* **1999**, *103*, 9966.
(24) Gerfen, G. J.; Hanna, P. A.; Chasteen, N. D.; Singel, D. J. *J. Am. Chem. Soc.* **1991**, *113*, 9513.
(25) Hamstra, b. J.; Houseman, A. L. P.; Colpas, G. J.; Kampf, J. W.; LoBrottu, R.; Frasch, W. D.; Pecoraro, V. L. *Inorg. Chem.* **1997**, *36*, 4866.
(26) LoBrutto, R.; Hamstra, B. J.; Colpas, G. J.; Pecoraro, V. L.; Frasch, W. D. *J. Am. Chem. Soc.* **1998**, *120*, 4410.
(27) Smith, T. S., II; Root, C. A.; Kampf, J. W.; Rasmussen, P. G.; Pecoraro, V. L. *J. Am. Chem. Soc.* **2000**, *122*, 767.
(28) Chen, W.; LoBrutto, R.; Frasch, W. D. *J. Biol. Chem.* **1999**, *274*, 7089.
(29) Cornman, C. R.; Zovinka, E. P.; Boyajian, Y. D.; Geiser-Bush, K. M.; Boyle, P. D.; Singh, P. *Inorg. Chem.* **1995**, *34*, 4213.
(30) Cornman, C. R.; Geiser-Bush, K. M.; Rowley, S. P.; Boyle, P. D. *Inorg. Chem.* **1997**, *36*, 6401.
(31) Grant, C. V.; Geiser-Bush, K. M.; Cornman, C. R.; Britt, R. D. *Inorg. Chem.* **1999**, *38*, 6285.
(32) Tolis, E. J.; Soulti, K. D.; Raptopoulou, C. P.; Terziz, A.; Deligiannakis, Y.; Kabanos, T. *Chem. Commun.* **2000**, 601.
(33) Petersen, J.; Hawkes, T. R.; Lowe, D. J. *J. Am. Chem. Soc.* **1998**, *120*, 10978.
(34) Makinen, M. W.; Mustafi, D. In *Metal Ions in Biological Systems*; Sigel, H., Sigel, A., Eds.; Marcel Dekker: New York, 1995; Vol. 31, p 89.
(35) Toy, A. D.; Chaston, S. H. H.; Pilbrow, J. R.; Smith, T. D. *Inorg. Chem.* **1971**, *10*, 2219.
(36) Press, W. H.; Teukolsky, S. A.; Vetterling, W. T.; Flannery, B. P. *Numerical Recipes in C*, 2nd ed.; Cambridge University Press: New York, 1992.
(37) Alderman, D. W.; Solum, M. S.; Grant, D. M. *J. Chem. Phys* **1986**, *84*, 3717.

(38) Velde, G. t.; Baerends, E. J. *J. Comput. Phys.* **1992**, *99*, 84.
(39) Versluis, L.; Ziegler, T. *J. Chem. Phys.* **1988**, *88*, 322.
(40) Schreckenbach, G.; Li, J.; Ziegler, T. *Int. J. Quantum Chem., Quantum Chem. Symp.* **1995**, *56*, 477.
(41) van Lenthe, E.; Wormer, P. E. S.; Avoird, A. v. d. *J. Chem. Phys* **1997**, *107*, 2488.
(42) van Lenthe, E.; Avoird, A. v. d.; Wormer, P. E. S. *J. Chem. Phys.* **1998**, *108*, 4783.
(43) van Lenthe, E.; Baerends, E. J.; Snijders, J. G. *J. Chem. Phys.* **1993**, *99*, 4597.
(44) van Lenthe, E.; Baerends, E. J.; Snijders, J. G. *J. Chem. Phys.* **1994**, *101*, 9783.
(45) van Lenthe, E.; Snijders, J. G.; Baerends, E. J. *J. Chem. Phys.* **1996**, *105*, 6505.
(46) van Lenthe, E.; Leeuwen, R. v.; Baerends, E. J.; Snijders, J. G. *Int. J. Quantum Chem.* **1996**, *57*, 281.
(47) van Lenthe, E.; Ehlers, A. E.; Baerends, E. J. *J. Chem. Phys.* **1999**, *110*, 8943.
(48) Vosko, S. H.; Wilk, L.; Nusair, M. *Can. J. Phys.* **1980**, *58*, 1200.
(49) Becke, A. D. *Phys. Rev. A.* **1988**, *38*, 3098.
(50) Perdew, J. P. *Phys. Rev. B.* **1986**, *33*, 8822.
(51) Petras, M.; Wichterlova, B. *J. Phys. Chem.* **1992**, *96*, 1805.
(52) Kevan, L.; Prakash, A. M. *J. Phys. Chem. B* **2000**, *104*, 6860.
(53) Wark, M.; Bruckner, A.; Liese, T.; Grunert, W. *J. Catal.* **1998**, *175*, 48.
(54) Martini, G.; Ottaviani, M. F.; Seravalli, G. L. *J. Phys. Chem.* **1975**, *79*, 1716.
(55) Balhausen, C. J.; Djurinskij, B. F.; Watson, K. J. *J. Am. Chem. Soc.* **1968**, *90*, 3305.
(56) Grant, C. V.; Cope, W.; Ball, J. A.; Maresch, G. G.; Gaffney, B. J.; Fink, W.; Britt, R. D. *J. Phys. Chem. B* **1999**, *103*, 10627.
(57) Mulks, C. F.; van Willigen, H. *J. Phys. Chem.* **1981**, *85*, 1220.
(58) Mulks, C. F.; Kirste, B.; van Willigen, H. *J. Am. Chem. Soc.* **1982**, *104*, 5906.
(59) van Willigen, H. *J. Magn. Reson.* **1980**, *39*, 37.
(60) van Willigen, H.; Chandrashekar, T. K. *J. Am. Chem. Soc.* **1983**, *105*, 4232.
(61) Larsen, S. C.; Singel, D. J. *J. Phys. Chem.* **1992**, *96*, 9007.
(62) Riejerse, E. J., Shane, J., de Boer, E.; Collison, D., Eds. *ESEEM of Nitrogen Coordinated Oxo-Vanadium(IV) Complexes*; World Scientific Publishers: Singapore City, 1989.
(63) Astashkin, A. V.; Dikanov, S. A.; Tsvetkov, Y. D. *J. Struct. Chem.* **1985**, *26*, 363.
(64) Knight, L. B., Jr.; Babb, R.; Ray, M.; Banisaukas, T. J., III; Russon, L.; Dailey, R. S.; Davidson, E. R. *J. Chem. Phys.* **1996**, *105*, 10237.
(65) Munzarova, M. L.; Kubacek, P.; Kaupp, M. *J. Am. Chem. Soc.* **2000**, *122*, 11900.
(66) Mattar, S., M.; Doleman, B. J. *Chem. Phys. Lett.* **1993**, *216*, 369.
(67) Albanese, N. F.; Chasteen, N. D. *J. Phys. Chem.* **1978**, *82*, 910.
(68) Atherton, N. M.; Shackleton, J. F. *Mol Phys.* **1980**, *39*, 1471.
(69) Francavilla, J.; Chasteen, N. D. *Inorg. Chem.* **1975**, *14*, 2860.
(70) Schneider, W. F.; Hass, K. C.; Ramprasad, R.; Adams, J. B. *J. Phys. Chem.* **1996**, *100*, 6032.
(71) Delabie, A.; Pierloot, K.; Groothaert, M. H.; Weckhuysen, B. M.; Schoonheydt, R. A. *Microporous Mesoporous Mater.* **2000**, *37*, 209.
(72) van Lenthe, E.; van der Avoird, A.; Hagen, W. R.; Reijerse, E. J. *J. Phys. Chem. A* **2000**, *104*, 2070.